Step-Edge-Induced Oxide Growth During the Oxidation of Cu Surfaces

Guangwen Zhou,[1,*] Langli Luo,[1] Liang Li,[1] Jim Ciston,[2,†] Eric A. Stach,[2] and Judith C. Yang[3]

[1]*Department of Mechanical Engineering and Multidisciplinary Program in Materials Science and Engineering, State University of New York at Binghamton, Binghamton, New York 13902, USA*

[2]*Center for Functional Nanomaterials, Brookhaven National Laboratory, Upton, New York 11973, USA*

[3]*Department of Chemical and Petroleum Engineering, University of Pittsburgh, Pittsburgh, Pennsylvania 15261, USA*

(Received 4 April 2012; revised manuscript received 18 August 2012; published 5 December 2012)

Using *in situ* atomic-resolution electron microscopy observations, we report observations of the oxide growth during the oxidation of stepped Cu surfaces. Oxidation occurs via direct growth of Cu_2O on flat terraces with Cu adatoms detaching from steps and diffusing across the terraces. This process involves neither reconstructive oxygen adsorption nor oxygen subsurface incorporation and is rather different from the mechanism of solid-solid transformation of bulk oxidation that is most commonly postulated. These results demonstrate that the presence of surface steps can promote the development of a flat metal-oxide interface by kinetically suppressing subsurface oxide formation at the metal-oxide interface.

DOI: 10.1103/PhysRevLett.109.235502 PACS numbers: 81.65.Mq, 68.37.Lp, 68.47.De

When exposed to an oxidizing environment, nearly all metals except Au will develop a surface oxide phase that is commensurate with the imposed environmental conditions. Such oxide formation plays an enormous role in technology, from causing serious corrosion problems, to providing protection against corrosive attack. The canonical description of oxide formation in metals involves a solid-solid transformation: during the initial stages of oxidation, the metal surface is assumed to undergo a series of structural changes starting with the initial oxygen chemisorption followed by oxygen subsurface incorporation resulting in conversion of the metal lattice into the oxide phase [1–20]; thereafter, at the later stages of oxidation, oxide scale growth involves incorporation of metal atoms at the metal-oxide interface and these solid-solid transformation processes require significant bulk diffusion of metal atoms to the surface or oxygen to the subsurface interface [21]. Such a mechanism has been inferred from idealized experiments that are primarily restricted to planar surfaces under ultrahigh vacuum (UHV) conditions. In practice, however, metallic surfaces are seldom perfect. Rather, they contain a high density of low-coordinated surface sites. Thus, in order to gain a detailed understanding of the mechanism of oxide formation under *realistic* conditions, the role of surface defects during surface oxidation must be elucidated under practical environments.

Transmission electron microscopy (TEM) has evolved dramatically in recent years and allows for temperature-, time-, and pressure-resolved imaging of oxidation at the atomic scale. This is accomplished by differentially pumped environmental TEM (max pressures of several Torr) and the incorporation of aberration correction techniques. Here we describe dynamic TEM observations of terraces and steps during the oxidation of Cu surfaces at the oxygen pressures that are many orders of magnitude higher than UHV experiments. By observing the coordinated step retraction and oxide propagation on terraces in real time we demonstrate that the oxidation process occurs via an adatom process, in which the bulk oxide phase grows on the surface terrace as a result of surface diffusion of adsorbed O atoms and Cu atoms detaching from step edges. This process does not involve the typical reaction sequence of reconstructive oxygen adsorption and subsurface oxygen incorporation and is significantly from a solid-solid transformation process.

The oxidation experiments were performed in a dedicated field-emission environmental TEM (FEI Titan 80–300) equipped with an objective-lens spherical aberration corrector. Using high-resolution TEM imaging, we can directly observe the evolution of the metal-oxide interface at the atomic scale at the elevated pressure and temperature. Cu(100) thin films with ~500 Å thickness were grown on NaCl(100) by *e*-beam evaporation and then removed from the substrate by floatation in deionized water and mounted on a TEM specimen holder. *In situ* TEM observations of the oxidation process were made in both planar and cross-sectional views. Observations in the cross section were made by imaging along faceted Cu edges of empty holes created *in situ* by deliberately annealing the Cu films at ~600 °C under H_2 gas flow to generate faceted cracks and holes. These fresh Cu edges generated in H_2 are oxide free and ideal for *in situ* TEM observations. Complete removal of the native oxide and surface cleanliness were confirmed by electron diffraction and electron energy loss spectroscopy.

Figure 1 presents *in situ* high-resolution transmission electron microscopy (HRTEM) images of a Cu(110) surface, seen edge-on at the oxygen pressure $p_{O_2} = 5 \times 10^{-3}$ Torr and $T = 350$ °C. In the range of T and p_{O_2} employed in our study, only Cu_2O is expected to form [13]. The oxidation proceeds through monolayer Cu_2O growth on the Cu(110) surface with $Cu_2O(110)//(Cu(110)$. The measured lattice spacing (~ 2.8 Å) indicates that the Cu_2O monolayer is under in-plane compression compared to bulk Cu_2O. The oxide growth starts from the upper-left corner and

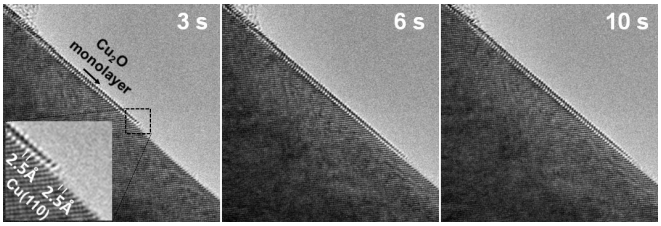

FIG. 1. *In situ* TEM observation of monolayer growth of Cu_2O on a nonreconstructed Cu(110) during the oxidation at 350 °C and $p_{O_2} = 5 \times 10^{-3}$ Torr (see *in situ* TEM movie **S1** in the Supplemental Material [29]). The lower-left inset is a zoom-in view of the oxide growth front revealing the nonreconstruction of the Cu(110) surface during the oxidation. The oxide growth occurs via an adatom mechanism, where adatoms of Cu are supplied from step edges and diffuse in across the Cu surface.

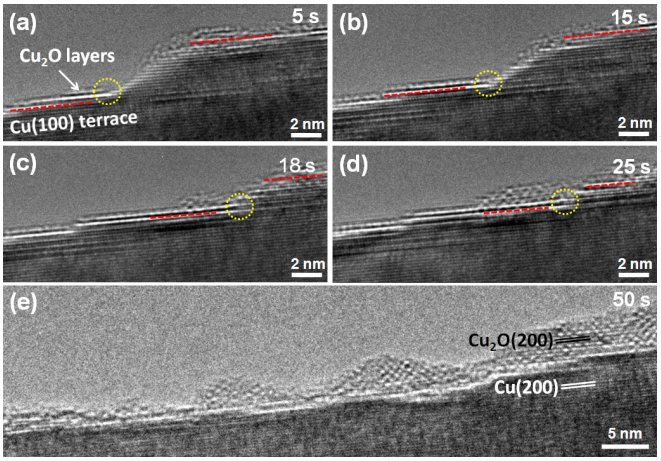

FIG. 2 (color online). (a)–(d) *In situ* TEM observations of the oxidation of Cu(100) terraces separated by a large step at 350 °C and $p_{O_2} = 5 \times 10^{-3}$ Torr (see *in situ* TEM movie **S2** in the Supplemental Material [29]). Dotted lines show the surface heights of the Cu_2O-Cu interfaces on the lower and upper terraces, and dotted circles show the formation of a misfit dislocation immediately at the step edge. Cu_2O layers are observed to grow laterally toward the step edge with the retraction of the Cu step, resulting in flattened Cu_2O-Cu interface. (e) Lower-magnification TEM image from the same area showing the 3D oxide island growth.

propagates rapidly along the surface. The *in situ* TEM images clearly show that the Cu_2O layer grows via an adatom mechanism, i.e., Cu and O atoms are added onto the growth front via surface diffusion, where Cu adatoms are released from low-coordinated surface sites such as step edges (not visible in this image). These observations also demonstrate that the oxidation does not involve reconstructive oxygen adsorption or oxygen subsurface incorporation as the Cu_2O layer grows. This is evidenced by the persistence of the intact structure of the Cu(110) surface, which experiences neither (2×1) nor $c(6 \times 2)$ restructuring such as has been observed during oxygen exposures in UHV environments [22–26]. At the (110) surface, the close-packed direction is along [110] with a lattice periodicity of 2.5 Å. The observed 2.5 Å periodicity along the [110] direction observed in Fig. 1 confirms that the Cu(110) surface did not reconstruct during the oxidation.

Figure 2 shows *in situ* HRTEM images, in a cross-sectional view along the [001] direction, of a Cu surface consisting of two (100) terraces separated by a large step, at $p_{O_2} = 5 \times 10^{-3}$ Torr and 350 °C. As can be clearly seen, Cu_2O nucleates on the (100) terrace at the terrace-step corner and propagates laterally. We see that the oxide forms directly on the (100) terrace and the oxide thickens via nucleation of new layers on the outer surface of the oxide, as evidenced by the intact and immobile terraces during the oxide growth. It is also apparent that the Cu_2O-Cu interface does not move into the terrace substrate during the oxidation. This suggests that the oxide growth observed here does not involve bulk diffusion of Cu and O atoms through the oxide layer, which would result in inward migration of the Cu_2O-Cu interface due to the metal-oxide transformation at the interface. In contrast, Cu atoms are supplied by step-edge detachment, as evidenced by the lateral propagation of the oxide layers toward the Cu step edge with the step retraction. This results in the formation of a new Cu_2O/Cu interface at the right-upper corner seen in Fig. 2(e). This is also evident by examining the evolution of the lateral distance between the left-lower and right-upper Cu_2O/Cu interfaces shown, respectively, in Figs. 2(a) and 2(d), where the immobile edge dislocation (dotted yellow circle) serves as a marker. In Fig. 2(a), the lateral distance between the two interfaces is about 5 nm, while it becomes about 2 nm in Fig. 2(d). This suggests that the right-upper Cu_2O/Cu interface seen in Fig. 2(d) is one that has newly formed due to the lateral growth of the oxide layer toward the Cu step [the upper-right Cu_2O/Cu interface appeared in Fig. 2(a) moved gradually out of the TEM field of view due to sample drift].

The coordinated lateral growth of the oxide and the retraction of Cu steps flatten the initially uneven Cu/Cu_2O interfaces. Figure 2(e) shows the overall morphology of the oxide layer after a period of oxidation. This image clearly indicates a 3D growth mode of the oxide. The resulting Cu_2O-Cu interface is relatively flat, despite of the initially large step height of the Cu surface. It is worth mentioning that the 3D oxide growth observed here is significantly different from 2D oxygen chemisorbed reconstruction [22–26] or 2D oxide film observed during the oxidation of atomically stepped surfaces under UHV gas dosing [27,28]. Our TEM observations show that nanometer-scale steps are capable of supplying a sufficient number of mobile Cu atoms for 3D oxide growth on the adjacent Cu terrace, a process similar as vapor deposition of a solid oxide. We examined the oxidation at p_{O_2} up to ~5 Torr (with the electron beam off), where a thicker oxide film with a similar flattened Cu-Cu_2O interface is observed (see Supplemental Material [29]). However, a significantly elevated oxygen pressure such as atmospheric pressure may result in immediate significant oxygen adsorption along surface steps, which may stabilize the step edge and lead to a change in the oxidation mechanism.

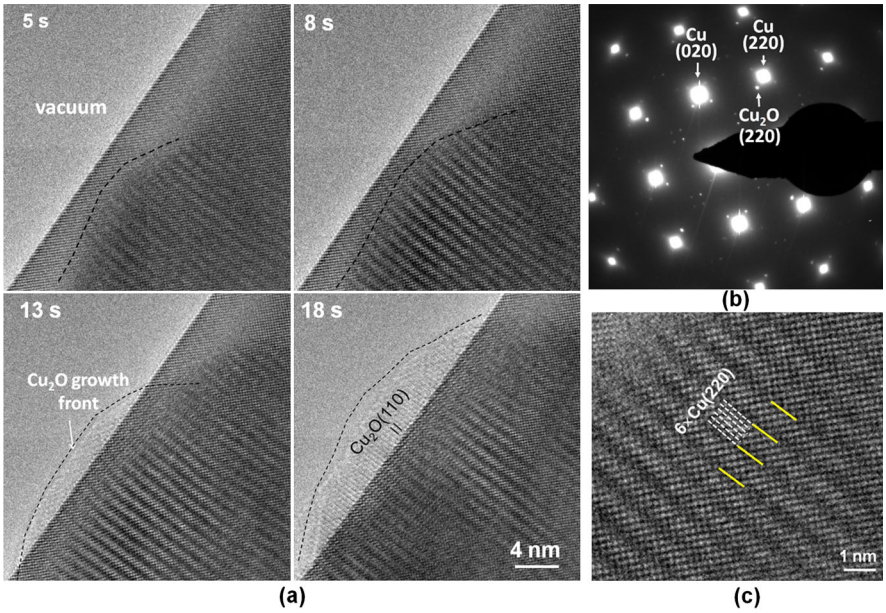

FIG. 3 (color online). (a) Time-resolved planar-view *in situ* TEM images showing the growth of a Cu_2O island on a Cu(100) surface during the oxidation at 350 °C and $p_{O_2} = 5 \times 10^{-3}$ Torr (see *in situ* TEM movie **S3** in the Supplemental Material [29]). The oxide island is observed to grow laterally initially on the surface then extending into the vacuum. (b) Selected area electron diffraction from an oxidized Cu(100) surface reveals the epitaxial growth of a Cu_2O island. (c) Enlarged view of *in situ* HRTEM image taken during the oxide growth, both the Cu(100) lattice fringes and moiré fringes are visible.

For comparison, we also examined flat surface areas far away step edges and noted that these flat regions are very stable under long-time electron beam illumination, suggesting the negligible effect of the electron beam irradiation on the oxide growth mode observed here.

Figure 3(a) presents *in situ* HRTEM images, in plan view, of the oxidation of a Cu(100) surface at $p_{O_2} = 5 \times 10^{-3}$ Torr and 350 °C. The moiré fringe contrast in the image is formed as a result of interference between diffracted beams from an overlapping Cu_2O lattice and the underlying Cu substrate lattice. In this imaging mode, it is not easy to discern surface steps, but the lateral propagation of the Cu_2O layer during oxidation provides clear evidence that the oxide growth is not occurring through a solid-solid transformation process. As seen from the *in situ* TEM images, the continued lateral growth of the oxide layer leads to its propagation into the empty hole. The measured lattice spacing of ~3.0 Å in this region corresponds to the lattice spacing of the $Cu_2O(110)$ plane, implying the continuation of the $Cu_2O(110)$ plane extending from the Cu surface. Since there is no ready source of Cu atoms in the vacuum region, growth of the oxide layer into the vacuum must call for delivery of Cu atoms across the oxide layer from the Cu film to the oxide growth front. It is thus evident that the oxide growth involves surface diffusion of Cu atoms created by detaching from step edges and oxygen atoms supplied from the vapor.

We then consider the effect of surface steps on the evolution of the metal-oxide interface. For a planar surface, the oxide grows via a solid-solid transformation process due to the lack of mobile metal atoms at the surface [1–20]. Stress caused by the molar volume mismatch between the oxide and the metal substrate plays a central role in determining the structural integrity of the metal-oxide interface. However, if large steps are present on the surface, the situation may be very different due to the availability of mobile metal atoms from steps. As seen in Fig. 2, oxide growth at the step edge results in a misfit dislocation immediately at the step edge, and the dislocation does not migrate during the subsequent oxide growth. This implies that the oxide growth involves no significant lattice stress at the metal-oxide interface.

This significantly reduced interface stress can be also verified from an analysis of the Cu_2O-Cu interface structure. Figure 3(b) is an electron diffraction pattern obtained from an oxidized Cu(100) surface. The two sets of diffraction spots can be indexed with the strong reflections from the Cu substrate and weak ones from the Cu_2O overlayer with the epitaxial relations of $[100]_{Cu_2O} \parallel [100]_{Cu}$ and $(220)_{Cu_2O} \parallel (220)_{Cu}$. Generally, the lattice constant of an oxide is significantly larger than that of the metal. The natural lattice misfit, $f = (a_{Cu_2O} - a_{Cu})/a_{Cu_2O}$, between Cu and Cu_2O is 15.4%. While epitaxial oxide growth occurs for many metal-oxide systems [30], the microscopic processes leading to the crystallographically aligned oxide growth for such large lattice-misfit systems is still very unclear, due primarily to the difficulty in obtaining dynamic atomic-scale information about the buried oxide-metal interface. A classic model used to describe the large-misfit epitaxy is coincidence site lattice (CSL) interface, which requires lattice strains be small enough to be energetically feasible for the heteroepitaxial growth.

In this case, the bilayer would be in a local minimum energy state if the mth atom of the overgrowth coincides with the nth atom of the substrate surface layer [31]. This condition is unrealistically restrictive, however. In real systems, the overlayer will tolerate a strain which is significantly smaller than the natural misfit between Cu_2O and Cu.

Moiré fringe contrast is sensitive to lattice strain and allows for the elucidation of interface structure [32]. Figure 3(c) presents an HRTEM image showing both moiré fringes and lattice fringes, viewed along the [001] axis. The moiré fringes run parallel to {220} planes of the Cu substrate, i.e., planes of the Cu_2O layer align with the substrate planes, both in equivalent {220} directions, consistent with the electron diffraction [Fig. 3(b)]. For moiré fringes generated by two sets of planes across an interface with spacing d_1 and d_2, the number of plane n of spacing d_2 between the moiré repeat is given by $n = d_2/(d_1 - d_2)$, where $d_1 > d_2$ [33]. Each repeat of the moiré fringes contains 6 Cu (220) planes. Substituting $n = 6$ and the lattice spacing of Cu(220) ($d_2 = 1.275$ Å), the interplanar spacing of the Cu_2O(220) (d_1) is determined to be 1.49 Å. This yields a lattice constant of $a_{Cu_2O} = 4.206$ Å. The number of {220} planes of Cu_2O in a moiré repeat is calculated as nd_2/d_1, which is 5. Thus, the growth of Cu_2O on the Cu(100) surface results in a (5×6) CSL epitaxy at the Cu_2O-Cu interface, i.e., every 5 {220} planes in the Cu_2O overlayer match 6 {220} planes of the Cu substrate, thereby experiencing a significantly reduced strain of ~1.48%. It is noted that such a CSL interface is initially not yet fully developed during the monolayer Cu_2O growth (Fig. 1), where the in-plane strain of the Cu_2O monolayer is ~7%, this is significantly larger than the lattice strain after developing into the (5×6) CSL interface for a thicker overlayer [Fig. 3(c)]. Such a trend is consistent with prior synchrotron x-ray measurements of the lattice strain of epitaxial Cu_2O films on Cu(111), which indicated that the in-plane lattice spacing approaches the bulk cuprite spacing as the oxide film grows thicker [34].

One expects oxygen subsurface diffusion with increased oxygen coverage if the mobility of substrate atoms is restricted, such as for a planar surface [1–20]. However, as shown from our observations, large surface steps provide sufficiently mobile metal atoms for direct oxide formation on the terrace without involving subsurface oxygen incorporation. A pictorial illustration of the oxide growth described above is given in Fig. 4. To give an indication of the size of the reaction barriers, we have used the nudged elastic band to calculate the diffusion barriers for the two possible reaction paths. For direct oxide formation on the terrace, the reaction can be limited by the surface diffusion of either Cu or O adatoms. Our *in situ* TEM observation (e.g., Fig. 1) shows that the un-oxidized Cu surface has an intact surface structure (no reconstructive oxygen adsorption) during the oxide growth. Meanwhile, the availability of mobile Cu adatoms from step edges can lead to fast annihilation of surface vacancies (if any) by Cu adatoms, a nonreconstructed Cu(100) surface is thus assumed for calculating the diffusion barriers of Cu and O adatoms. The calculated energy barriers for Cu and O adatoms hopping between fcc hollow sites via a minimum energy path passing through the bridge site are ~0.50 and 0.71 eV, respectively. However, if the solid-solid transformation occurs, oxygen must diffuse into the subsurface region. Earlier DFT studies have shown that the diffusion barrier for O penetration below the surface depends on the O surface coverage on the missing-row reconstructed Cu surface [13–15,20,35–37]. In our DFT calculations, a nonreconstructed Cu(100) surface is used and the calculated diffusion barrier is ~1.71 eV for 0.5 monolayer oxygen coverage (see Supplemental Material [29]). The significantly higher barrier for oxygen subsurface diffusion explains the observations that oxide formation via surface diffusion of Cu and O adatoms is kinetically more favorable.

We finally discuss the effect of surface steps on the longer-term oxidation of a metal surface. Flat surfaces are usually desired in obtaining smooth interfaces during heteroepitaxy. However, for the oxidation of an atomically flat metal surface, subsurface incorporation of oxygen results in significant interfacial stress due to the large volume expansion which occurs upon transformation of the metal lattice into its oxide. This can lead to instability of a planar interface [38] and may even cause mechanical breakdown at the metal-oxide interface [39]. In contrast, the presence of large steps kinetically suppresses oxygen subsurface embedment and is actually beneficial to the formation of improved metal-oxide interfaces, for both interface flatness and mechanical integrity. We observe that oxidation of the stepped surface results in unconstrained oxide growth with a relatively flat Cu_2O-Cu interface via depletion of Cu atoms from surface steps. The enhanced interface flatness can provide better protection to the underlying metal substrate. As revealed in Fig. 2, the Cu_2O-Cu interface is immobile during the oxide thickening because the intact Cu_2O-Cu interface restricts transfer of Cu atoms from the underlying Cu substrate into the oxide. Accordingly,

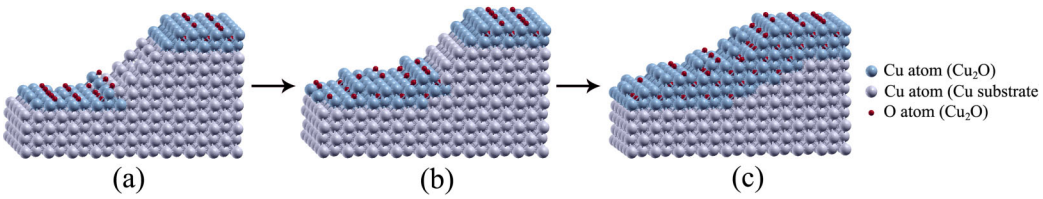

FIG. 4 (color online). Pictorial illustration of the step-edge induced oxide growth. Oxide layers grow laterally toward the step edge with retraction of the Cu step, whereby flattening initially uneven Cu_2O-Cu interfaces.

although stepped surfaces usually have enhanced reactivity toward initial oxide formation due to enhanced mobility of surface atoms, the longer-term oxidation kinetics may be slower than for flat surfaces because of the formation of an improved metal-oxide interface.

In summary, we have observed in real time the behavior of terraces and steps during oxidation. Our *in situ* TEM visualization reveals that surface steps are the dominant source of Cu adatoms for oxide growth on surface terraces, a mechanism which does not involve reconstructive oxygen adsorption and oxygen subsurface incorporation and which suggests the formation of improved flatness of the metal-oxide interface with significantly reduced interfacial stress. Acquiring the ability to control the microscopic processes governing the surface oxidation has huge technological implications; the results described here may have broader impact for manipulating metal oxidation to affect oxidation kinetics via controlling the surface morphology.

This work was supported by the U.S. Department of Energy, Office of Basic Energy Sciences, Division of Materials Sciences and Engineering under Award No. DE-FG02-09ER46600. Research carried out in part at the Center for Functional Nanomaterials, Brookhaven National Laboratory, which is supported by the U.S. Department of Energy, Office of Basic Energy Sciences, under Contract No. DE-AC02-98CH10886. This work used the Extreme Science and Engineering Discovery Environment (XSEDE), which is supported by National Science Foundation Grant No. OCI-1053575.

*To whom correspondence should be addressed.
gzhou@binghamton.edu
†Present address: National Center for Electron Microscopy, Lawrence Berkeley National Laboratory, Berkeley, CA 94720, USA.

[1] K. R. Lawless, Rep. Prog. Phys. **37**, 231 (1974).
[2] C. I. Carlisle, T. Fujimoto, W. S. Sim, and D. A. King, Surf. Sci. **470**, 15 (2000).
[3] M. Todorova, W. X. Li, M. V. Ganduglia-Pirovano, C. Stampfl, K. Reuter, and M. Scheffler, Phys. Rev. Lett. **89**, 096103 (2002).
[4] J. Gustafson, A. Mikkelsen, M. Borg, E. Lundgren, L. Köhler, G. Kresse, M. Schmid, P. Varga, J. Yuhara, X. Torrelles, C. Quirós, and J. N. Andersen, Phys. Rev. Lett. **92**, 126102 (2004).
[5] M. Todorova, K. Reuter, and M. Scheffler, Phys. Rev. B **71**, 195403 (2005).
[6] H. Bluhm, M. Havecker, A. Knop-Gericke, M. Kiskinova, R. Schlögl, and M. Salmeron, MRS Bull. **32**, 1022 (2007).
[7] P. Dudin, A. Barinov, L. Gregoratti, M. Kriskinova, F. Esch, C. Dri, C. Africh, and G. Comelli, J. Phys. Chem. B **109**, 13 649 (2005).
[8] G. Ketteler, D. F. Ogletree, H. Bluhm, H. J. Liu, E. L. D. Hebenstreit, and M. Salmeron, J. Am. Chem. Soc. **127**, 18 269 (2005).
[9] N. Al-Sarrafa, J. T. Stucklessa, C. E. Wartnaby, and D. A. King, Surf. Sci. **283**, 427 (1993).
[10] U. Starke, M. A. Van Hove, and G. A. Somorjai, Prog. Surf. Sci. **46**, 305 (1994).
[11] W. A. Brown, R. Kose, and D. A. King, Chem. Rev. **98**, 797 (1998).
[12] J. T. Stuckless, C. E. Wartnaby, N. Al-Sarraf, S. J. Dixon-Warren, M. Kovar, and D. A. King, J. Chem. Phys. **106**, 2012 (1997).
[13] X. Duan, O. Warschkow, A. Soon, B. Delley, and C. Stampfl, Phys. Rev. B **81**, 075430 (2010).
[14] M. Y. Lee and A. J. H. McGaughey, Surf. Sci. **603**, 3404 (2009).
[15] M. Y. Lee and A. J. H. McGaughey, Surf. Sci. **604**, 1425 (2010).
[16] R. Blume, H. Niehaus, H. Conrad, A. Bottcher, L. Aballe, L. Gregoratti, A. Barinov, and M. Kiskinova, J. Phys. Chem. B **109**, 14 052 (2005).
[17] A. Soon, M. Todorova, B. Delley, and C. Stampfl, Phys. Rev. B **73**, 165424 (2006).
[18] Y. B. He, A. Stierle, W. X. Li, A. Farkas, N. Kasper, and H. Over, J. Phys. Chem. C **112**, 11 946 (2008).
[19] K. Reuter, C. Stampfl, M. V. Ganduglia-Pirovano, and M. Scheffler, Chem. Phys. Lett. **352**, 311 (2002).
[20] L. Li, X. Mi, Y. F. Shi, and G. W. Zhou, Phys. Rev. Lett. **108**, 176101 (2012).
[21] C. Wagner, Z. Phys. Chem., Abt. B **21**, 25 (1933).
[22] D. J. Coulman, J. Wintterlin, R. J. Behm, and G. Ertl, Phys. Rev. Lett. **64**, 1761 (1990).
[23] F. Jensen, F. Besenbacher, E. Lasgaard, and I. Stensgaard, Phys. Rev. B **41**, 10233 (1990).
[24] R. Feidenhansl, F. Grey, M. Nielsen, F. Besenbacher, F. Jensen, E. Laegsgaard, I. Stensgaard, K. W. Jacobsen, J. K. Norskov, and R. L. Johnson, Phys. Rev. Lett. **65**, 2027 (1990).
[25] K. Kern, H. Niehaus, A. Schatz, P. Zeppenfeld, J. Goerge, and G. Comsa, Phys. Rev. Lett. **67**, 855 (1991).
[26] L. Guillemot and K. Bobrov, Phys. Rev. B **83**, 075409 (2011).
[27] M. Eumann, G. Schmitz, and R. Franchy, Appl. Phys. Lett. **72**, 3440 (1998).
[28] R. Franchy, Surf. Sci. Rep. **38**, 195 (2000).
[29] See Supplemental Material at http://link.aps.org/supplemental/10.1103/PhysRevLett.109.235502 for *in situ* TEM movies and DFT calculations of energy barriers.
[30] M. Gebhardt and A. Neuhaus, *Landolt-Bornstein: Epitaxial Data of Inorganic and Organic Crystals* (Springer-Verlag, New York, 1972).
[31] J. W. Matthews, in *Epitaxial Growth*, Part B, edited by J. W. Matthews (Academic Press, New York, 1975).
[32] D. B. Williams and C. B. Carter, *Transmission Electron Microscopy* (Plenum, New York, 1996).
[33] P. B. Hirsch, A. Howie, R. B. Nicholson, D. W. Pashley, and M. J. Whelan, *Electron Microscopy of Thin Crystals* (Krieger, New York, 1977).
[34] Y. S. Chu, I. K. Robinson, and A. A. Gewirth, J. Chem. Phys. **110**, 5952 (1999).
[35] A. Soon, M. Todorova, B. Delley, and C. Stampfl, Surf. Sci. **601**, 5809 (2007).
[36] T. Kangas and K. Laasonen, Surf. Sci. **602**, 3239 (2008).
[37] T. Kangas, K. Lassonen, A. Puisto, H. Pitkanen, and M. Alatalo, Surf. Sci. **584**, 62 (2005).
[38] G. Grinstein, Y. H. Tu, and J. Tersoff, Phys. Rev. Lett. **81**, 2490 (1998).
[39] H. E. Evans, Int. Mater. Rev. **40**, 1 (1995).